Responses of marginal and intrinsic water-use efficiency to changing aridity using FLUXNET observations

Koong Yi[1], Kimberly A. Novick[2], Quan Zhang[3], Lixin Wang[4], Taehee Hwang[5], Xi Yang[6], Kanishka Mallick[7,8], Martin Béland[7,9], Gabriel B. Senay[10], Dennis Baldocchi[7]

[1]Earth and Environmental Sciences Area, Lawrence Berkeley National Laboratory, CA, U.S.A.

[2]O'Neill School of Public and Environmental Affairs, Indiana University Bloomington, Bloomington, IN, U.S.A.

[3]State Key Laboratory of Water Resources and Hydropower Engineering Science, Wuhan University, Wuhan, China.

[4]Department of Earth Sciences, Indiana University-Purdue University Indianapolis (IUPUI), Indianapolis, IN, U.S.A.

[5]Department of Geography, Indiana University Bloomington, Bloomington, IN, U.S.A.

[6]Department of Environmental Sciences, University of Virginia, Charlottesville, VA, U.S.A.

[7]Department of Environmental Science, Policy, and Management, University of California, Berkeley, CA, U.S.A.

[8]Department of Environment Research and Innovation, Luxembourg Institute of Science and Technology, Belvaux, Luxembourg

[9]Department of Geomatics Sciences, Laval University, Quebec City, Quebec, Canada

[10]U.S. Geological Survey Earth Resources Observation and Science Center, North Central Climate Adaptation Science Center, Fort Collins, CO, U.S.A.

Corresponding Author:
Koong Yi
Email: koongyi@gmail.com
Phone: +1-812-650-2930

Abstract

According to classic stomatal optimization theory, plant stomata are regulated to maximize carbon assimilation for a given water loss, and a key component of stomatal optimization models is marginal water-use efficiency (mWUE). While the mWUE is often assumed to be constant, variability of mWUE under changing hydrologic conditions has been reported. However, there has yet to be a consensus on the patterns of mWUE variabilities and their relations with atmospheric aridity. We investigate the dynamics of mWUE in response to vapor pressure deficit (VPD) and aridity index using carbon and water fluxes from 115 eddy covariance towers available from the global database FLUXNET. We demonstrate a non-linear mWUE-VPD relationship at a sub-daily scale in general; mWUE varies significantly at both low and high VPD levels. However, mWUE remains relatively consistent within the mid-range of VPD. Despite the highly non-linear relationship between mWUE and VPD, the relationship can be informed by the strong linear relationship between ecosystem-level inherent water-use efficiency (IWUE) and mWUE using the slope, m^*. We further identify site-specific m^* and its variability with changing site-level aridity across six vegetation types. We suggest accurately representing the relationship between IWUE and VPD using non-linear functions, such as Michaelis-Menten or quadratic functions, to ensure precise estimation of mWUE variability for individual sites.

Plain Language Summary

Plants employ diverse strategies for water utilization during growth. Marginal water-use efficiency (mWUE) quantifies how effectively plants assimilate carbon relative to the water they lose through transpiration. A scientific debate exists regarding how mWUE responds to dry conditions. To investigate this, we analyze data from various vegetation types worldwide, observing changes in mWUE under dry conditions. Contrary to common assumptions, mWUE is not a constant; it varies significantly based on moisture levels. Additionally, we show that a simpler measure called inherent water-use efficiency (IWUE) can help explain this complicated relationship, which is useful for predicting plant growth under different moisture conditions.

Keywords

Climate change, drought, eddy covariance, FLUXNET, stomatal optimization theory, vapor pressure deficit, water-use efficiency

Running title

Response of mWUE and IWUE to changing aridity

1. Introduction

Terrestrial plants mitigate global warming by sequestering atmospheric carbon dioxide (CO_2) through photosynthesis (Beer et al., 2010). However, photosynthesis is inherently linked with plant water loss via transpiration, as CO_2 and water vapor share the same stomatal pathway. Plants risk hydraulic damage during droughts if they maintain high stomatal conductance as soil water availability decreases and atmospheric demand increases, resulting in low leaf water potential and xylem cavitation. Therefore, plants must balance stomatal function to optimize carbon uptake while minimizing transpirational water loss and hydraulic stress (Cowan & Farquhar, 1977; Katul et al., 2010; Sperry et al., 2017; Wang et al., 2020). To predict plant ecophysiological responses to projected changes in atmospheric CO_2 concentration, elevated atmospheric water demand, and more severe and frequent drought events, we need a mechanistic understanding of how different ecosystems regulate the trade-off between photosynthetic carbon assimilation and transpirational water loss.

While carbon uptake is usually represented through mechanistic models of photosynthesis (e.g., the Michaelis-Menten equation (Michaelis & Menten, 1913; Marshall & Biscoe, 1980; Thornley, 1998); the Farquhar model (Von Caemmerer, 2000; Farquhar et al., 1980a)), water use (i.e., transpiration) is often described based on empirical relationships that prescribe how stomatal conductance responds to environmental drivers and carbon uptakes. For example, the Ball-Berry model (Ball et al., 1987) is one of the most widely used empirical stomatal conductance models (Anderegg et al., 2017; Buckley, 2017; Katul et al., 2010), and has been readily incorporated into many climate models (Bonan et al., 2014). It takes the form:

$$g_s = g_0 + g_1 \frac{A}{c_a} RH \qquad (1)$$

where g_s is stomatal conductance (mol m^{-2} s^{-1}), A is carbon assimilation rate (μmol m^{-2} s^{-1}), c_a is atmospheric CO_2 concentration (ppm), RH is relative humidity at the leaf surface, and g_0 and g_1 are empirically fitted parameters. To simulate the non-linear variation in g_s with changing humidity, Leuning (1995) modified the Ball-Berry model by replacing relative humidity with a vapor pressure deficit (VPD) response function as follows:

$$g_s = g_0 + g_1 \cdot \frac{A}{(c_a - \Gamma^*)\left(1 + \frac{VPD}{VPD_0}\right)} \qquad (2)$$

where Γ^* is CO_2 compensation point for photosynthesis (ppm) and VPD_0 is the empirically determined coefficient, representing the slope of the relationship between g_s and VPD. These empirical models are relatively simple, easy to use, and work well for well-watered conditions (Bonan et al., 2014). However, they have an incomplete grounding in physiological theory, leading to uncertainty when they are extrapolated to predict plant function under unprecedented climate conditions (Franks et al., 2018; Knauer et al., 2015, 2018; Medlyn et al., 2012; Sabot et al., 2022).

An alternative way to enable the theoretical interpretation of leaf-level stomatal conductance models is to adopt the principle of stomatal optimization theory (Anderegg et al., 2018; Bonan et al., 2014; Katul et al., 2009; Katul et al., 2010; Medlyn et al., 2012; Novick et al., 2016b; Sperry et al., 2017; Wolf et al., 2016). Stomatal optimization theory was originally based on a hypothesis that stomata are regulated to maximize carbon assimilation (A) for a given water loss (transpiration, E). A key parameter in this class of models is the so-called "marginal water-use efficiency (mWUE)," here defined as the ratio of a change in E to a change in A ($\partial E/\partial A$) following Cowan and Farquhar (1977), though it is sometimes defined as the inverse form ($\partial A/\partial E$) (Katul et al., 2010; Manzoni et al., 2011). The optimality models often maintain the mWUE constant over arbitrary time steps (e.g., daily), assuming abundant water at the canopy

(Buckley, 2017; Cowan & Farquhar, 1977; Makela et al., 1996). However, this may not hold true at sub-daily timescales, where high atmospheric demand (i.e., VPD) during midday can decrease water potential at the canopy level even when soil moisture is abundant (Anderegg et al., 2017; Grossiord et al., 2020).

Understanding how mWUE changes under hydrologic stress is necessary for the optimization models in a prognostic sense, yet no consensus on the magnitude or even direction of these changes exists. For instance, Manzoni et al. (2011) and Zhou et al. (2013, 2014) performed meta-analyses of leaf gas exchange measurements from previous studies that spanned wide ranges of species and moisture conditions. A major difference in their approaches was the proxy for plant water status; Manzoni et al. (2011) used mid-day leaf water potential, while Zhou et al. (2013, 2014) used pre-dawn leaf water potential as a proxy for soil moisture availability. Similarly, Lin et al. (2015) compiled a global database of leaf gas exchange measurements spanning diverse plant functional types and estimated a slope parameter (g_1) (Medlyn et al., 2012), which is analogous to the slope parameter from empirical models (Eqs. 1 & 2) and proportional to $\sqrt{\partial E/\partial A}$ (Medlyn et al., 2012). They further evaluated the relationship between g_1 and a moisture index, defined as the ratio of mean annual precipitation to the equilibrium evapotranspiration. Mäkelä et al. (1996) and Lu et al. (2016) took a theoretical approach to examine short- and long-term optimal stomatal behavior, respectively, in response to the soil moisture availability assuming that plants are adapted to the stochastic rainfall patterns of their environments. More recently, alternative stomatal optimization perspectives have been proposed, which presume stomata function to maximize carbon uptake while minimizing water costs, including those linked to hydraulic damage during droughts (Anderegg et al., 2018; Sperry et al., 2017; Wolf et al., 2016). While promising, in contrast to the Medlyn et al. (2012) model, these

newer formulations have yet to be integrated into land surface model schemes (but see Kennedy et al., 2019, for a study implementing plant hydraulics in the Community Land Model). While theoretical expectation and many studies suggest decreasing mWUE as water stress drives reductions to g_s, there is some evidence of increasing mWUE under water stress (Farquhar et al., 1980b; Grieu et al., 1988; Zhou et al., 2013), although reasons for this needed to be clarified.

It is also important to note that canopy water status and water potential are not determined solely by the availability of water supply but by the balance between water supply and demand, with VPD as a major force exerted on the canopy by the atmosphere (Manzoni et al., 2011, 2013; Novick et al., 2019). Thus, it is reasonable to expect that mWUE must be adjusted with changing atmospheric water demand unless other factors limit the plant response (e.g., compromised hydraulic conductivity under water stress, limited soil moisture availability to plants) (Brodribb et al., 2005; Medlyn et al., 2012). Different plants or ecosystems may adjust differently, resulting in divergent responses of mWUE to changing VPD. Understanding the relationship between mWUE and VPD is important given that VPD is expected to keep increasing in the future, which will exert further water stress on plants (Ficklin & Novick, 2017; Grossiord et al., 2020; Novick et al., 2016a; Zhang et al., 2019). Furthermore, while soil moisture is a stochastic variable due to its dependency on intermittent rainfall, VPD is smoother in time and easier to monitor through various meteorological or gas exchange measurement techniques. Although VPD and soil moisture limit plants' carbon uptake and water use independently (Yi et al., 2019), VPD can be used as a proxy of water stress at a sub-daily scale where VPD plays a primary role in regulating stomatal regulation unless severe soil moisture deficiency, as suggested by the models with sub-daily timesteps (e.g., Ball-Berry model and its variations), and in turn influencing the balance between carbon uptake and water loss (i.e., water-

use efficiency) at a sub-daily scale (Baldocchi et al., 2022; Grossiord et al., 2020; Novick et al., 2016a). Therefore, examining the association between mWUE and VPD would add insight into the predictability of soil moisture alone.

The objectives of this study are 1) to investigate the variation of mWUE at an hourly timescale in response to changing VPD and 2) to explore approaches for estimating mWUE explicitly from the modeled relationship between intrinsic water-use efficiency (iWUE, carbon assimilation per unit stomatal conductance, representing water-use efficiency at leaf level) and VPD. The Ball-Berry model (Eq. 1) reveals that the parameter g_1, which is proportional to $\sqrt{\partial E/\partial A}$ (Medlyn et al., 2012), is related to A/g_s (= iWUE at leaf level). The iWUE can be more straightforwardly estimated from field measurements across various spatiotemporal scales, including leaf gas exchange (daily to weekly at the leaf level), dendrochronology (seasonal/annual at the tree level), and eddy covariance (hourly at the stand level) (see more discussion on iWUE at different scales from Beer et al., 2009 and Yi et al., 2019). Notably, the inference of iWUE from tree-ring analyses provides an avenue for understanding historical variations in iWUE and, potentially, mWUE. While iWUE has a mathematically simpler form and thus facilitates modeling its response to water stress, the complex mathematical expression of mWUE poses challenges in generalizing its variability at a sub-daily timescale. By elucidating the correlation between iWUE and mWUE, we can gain insights into the response of mWUE to water stress. Additionally, through site comparisons, we further explore whether there is an emerging pattern in the correlation between iWUE and mWUE across different vegetation types and aridity levels.

Table 1. A glossary of terms related to water-use efficiency.

Term or symbol	Definition
A	Carbon assimilation rate
c_a	Atmospheric CO_2 concentration
E	Transpiration rate
ET	Evapotranspiration rate
g_0	Intercept parameter in Ball-Berry model (represents minimum leaf conductance)
g_1	Slope parameter in Ball-Berry model (represents marginal water-use efficiency, mWUE)
g_s	Stomatal conductance
GPP	Gross primary productivity
iWUE	Intrinsic water-use efficiency; leaf-level water-use efficiency (= A / g_s)
IWUE	Inherent water-use efficiency; a proxy of intrinsic water-use efficiency at the ecosystem level (= GPP × VPD / ET / P_a, Beer et al., 2009)
mWUE	Marginal water-use efficiency, the ratio of a change in E to a change in A ($= \partial E/\partial A$)
P_a	Atmospheric pressure
VPD	Vapor pressure deficit

178

179 # 2. Materials and Methods

180 ## 2.1. FLUXNET data

181 We obtained half-hourly measurements of carbon and energy fluxes, along with ancillary
182 environmental data, from 115 flux towers across FLUXNET sites. These data were collected
183 using the FLUXNET 2015 Tier 1 database (Table S1) (Pastorello et al., 2020). Eddy covariance
184 records, which have the benefit of providing continuous meteorological and gas exchange data at
185 the high temporal resolution, are very well suited for investigating the relationship between gas
186 exchange dynamics, mWUE, and VPD at the ecosystem scale.

187 We selected the study sites from six vegetation types (grassland, cropland, shrubland,
188 savanna, broadleaf forest, and needleleaf forest, based on the IGBP land cover classification

system) based on the data availability for the variables required for the analysis. For reliable and clear mWUE analysis, we only included the sites that had at least three years of data and a strong iWUE-VPD correlation. Specifically, we selected the sites that had $R^2 > 0.8$ with any of the three model fits – linear, quadratic, or Michaelis-Menten –, which was the case for more than 70% of the sites over three years of data (See section 2.4 for more information about the model fits). In addition, we only used the data where net ecosystem exchange (NEE), latent heat flux (LE), and sensible heat flux (H) were either original measurements (quality control flag = 0) or gap-filled data of good quality (quality control flag = 1) to ensure data quality and make the most of the data. We only used daytime data when net radiation was greater than 0 W m^{-2} without precipitation. We also limited our analysis to the growing season, where daily GPP was larger than 10% of the 95th percentiles of daily GPP for each site with > 5°C air temperature. We used the GPP partitioned based on the standard daytime method (variable name: GPP_DT_VUT_REF, Lasslop et al., 2010). Additional filtering criteria were applied for some key variables: atmospheric CO_2 concentration between 350 ppm and 420 ppm, friction velocity (u^*) greater than 0.1 m s^{-1}, and canopy conductance calculated by Penman-Monteith equation (Monteith, 1965) greater than 0.05 mol m^{-2} s^{-1}. Lastly, we removed outliers of the environmental drivers and biological variables (i.e., air temperature, relative humidity, atmospheric CO_2 concentration, latent heat flux, wind speed, VPD, atmospheric pressure, friction velocity, net radiation, soil water content, canopy conductance, iWUE, and mWUE) by excluding data that were below the 5th or above the 95th percentiles of each variable. Note that the purpose of data filtering was to remove exceptionally low or high values of the variables, which we consider outliers. Our goal was to ensure that the results, especially the variability of mWUE, were not

unduly influenced by these outliers. We carefully examined the histograms for the variables for each site to minimize data reduction while retaining useful information.

2.2. Two different approaches describing mWUE

We used two different approaches for describing the mWUE: two optimization-theory-driven mWUE, the solution of "$\partial E/\partial A$" suggested by Katul et al. (2010) and the "g_1" parameter proposed by Medlyn et al. (2012). The difference between the optimization-theory-driven mWUE is based on their interpretation of stomatal optimization. Katul et al. (2010) assumed that stomata are optimizing for photosynthesis limited by Rubisco activity (i.e., carbon-limited), and plant stomatal optimality is subject to change (i.e., mWUE is not constant). On the other hand, Medlyn et al. (2012) assumed that stomata are optimized for photosynthesis limited by RuBP-regeneration (i.e., light-limited). In either case, the optimization objective should result in constant mWUE values at short timescales – Katul et al. (2010) suggested approximately 10 minutes, while Medlyn et al. (2012) suggested daily or longer – although it may change at longer timescales as hydrologic conditions evolve.

Following Katul et al. (2010), the $\partial E/\partial A$ emerges from an optimality condition determined with a linearized variant of the Farquhar et al. (1980) photosynthesis model, defined as:

$$\frac{\partial E}{\partial A} = 1.6\, VPD\, c_a \left(\frac{A}{g_s}\right)^{-2} = \frac{1.6\, VPD\, c_a}{iWUE^2} \qquad (3)$$

where iWUE is defined as a ratio of A to g_s at the leaf-scale (Beer et al., 2009).

The other perspective on optimality proposed by Medlyn et al. (2012) takes an analogous form to an empirical model proposed by Leuning (1995) (Eq. 2):

$$g_s \approx g_0 + 1.6\left(1 + \frac{g_1}{\sqrt{VPD}}\right)\frac{A}{c_a} \qquad (4)$$

234 This approach suggests that the parameter g_1 represents a slope between g_s and $A/c_a\sqrt{VPD}$ and
235 is proportional to $\sqrt{\partial E/\partial A}$ (Lin et al., 2015; Medlyn et al., 2012). Therefore, to facilitate
236 comparison between the two approaches, we compare $\partial E/\partial A$ with squared g_1 (i.e., g_1^2) in
237 throughout the results. Eq. 4 was rearranged with an assumption that g_0, which represents
238 cuticular conductance to water vapor, is negligible (but see Manzoni et al. (2011) and Lanning et
239 al. (2020) for discussion of the role of cuticle conductance under drier conditions):

240 $$g_1 = \left(\frac{g_s\, c_a}{1.6\, A} - 1\right)\sqrt{VPD} = \left(\frac{c_a}{1.6\, iWUE} - 1\right)\sqrt{VPD} \qquad (5)$$

241 Consequently, two different mWUE parameters, $\partial E/\partial A$ (mol $H_2O \cdot kPa \cdot mol^{-1}$ of dry air) and g_1
242 (mol $H_2O \cdot kPa^{0.5} \cdot mol^{-1}$ of dry air), were expressed as functions of iWUE, c_a, and VPD.
243 Assuming c_a is relatively stable over a short period, we focus on how iWUE (as a biological
244 factor) and VPD (as an indicator of water stress governing plant response at a short temporal
245 scale, e.g., sub-daily) affect both mWUE parameters (more details discussed in section 2.5). We
246 applied an approximation of iWUE at the ecosystem level, inherent WUE (IWUE), defined by
247 Beer et al. (2009). IWUE (μmol C mol^{-1} H_2O) was particularly suitable for our study because
248 IWUE can be calculated from the measurements of carbon and water fluxes by eddy covariance
249 technique and ancillary meteorological data, i.e., GPP (μmol m^{-2} s^{-1}) from net ecosystem
250 exchange representing canopy-level carbon assimilation, evapotranspiration rate (ET, mol m^{-2} s^{-1}) from latent heat flux, VPD under the assumption of equal temperatures of leaves and
252 atmosphere, and atmospheric pressure (P_a, kPa):

253 $$IWUE = \frac{GPP \cdot VPD}{ET \cdot P_a} \qquad (6)$$

254

255 Several important assumptions for the definition of IWUE include (1) small and invariant soil
256 evaporation (E) compared to plant transpiration (T) over the course of the day (hence $\Delta ET \sim \Delta T$)

especially during days without rainfall (conditions we used for our analysis), (2) thermal equilibrium between leaf and air, which influences VPD, and (3) disregarding of aerodynamic resistance through the boundary layer that can change depending on the vegetation structure (See Beer et al. (2009) for more discussion about IWUE as a proxy of ecosystem-level intrinsic WUE). We confirmed the robustness of IWUE as a proxy of iWUE at the ecosystem level by comparing it with a few other definitions of iWUE (the comparison results are available in the Supporting information; Figs. S1 & S2). Note that IWUE and mWUE were computed using half-hourly FLUXNET data; hence, their variabilities discussed here represent plant physiological response at a sub-hourly scale.

2.3. Sensitivity of mWUE parameters to moisture condition

Variations of mWUE parameters in response to moisture conditions (i.e., atmospheric water demand and site-level aridity) were evaluated at the individual site level and across sites. For the individual sites, mWUE parameters were partitioned into discrete bins spanning a range of VPD. To avoid biases from unevenly distributed data points across the range of VPD (i.e., sample sizes at low and high VPD are smaller than those for the intermediate level of VPD), data binning was performed in a way that the sample sizes were evenly distributed into 30 bins across the range of VPD at each site. Then, mWUE-VPD relationships were produced based on the mean mWUE values generated for the different VPD bins.

To compare across the sites, the relationships between site-specific mWUE and aridity index (AI) were evaluated (See Fig. S3 in the Supporting Information for AI at all the study sites). AI was defined as the ratio of annual precipitation (P) to annual potential evapotranspiration (PET) and averaged over the observation period for each site (UNEP, 1992):

$$AI = \frac{P}{PET} \qquad (7)$$

The annual PET was determined by summing up the half-hourly PET values over the course of a year, employing the FAO Penman-Monteith method as outlined by Allen et al. (1998):

$$PET = \frac{0.408\Delta(R_n - G) + \gamma \frac{900}{T_a + 273} u(e_s - e_a)}{\Delta + \gamma(1 + 0.34u)} \qquad (8)$$

where Δ is the slope of vapor pressure curve (kPa $℃^{-1}$), R_n is the net radiation (MJ m^{-2} hr^{-1}), G is the soil heat flux density (MJ m^{-2} hr^{-1}), γ is the psychrometric constant (kPa $℃^{-1}$), T_a is the air temperature (℃), u is the wind speed (m s^{-1}), e_s is the saturation vapor pressure (kPa), and e_a is the actual vapor pressure (kPa). The estimation of AI is sensitive to gaps in precipitation data. Therefore, we used long-term mean annual precipitation provided on the site information page at the FLUXNET website rather than calculating mean annual precipitation from the FLUXNET2015 dataset. For the sites where annual precipitation records were not provided, the high-frequency precipitation record in the FLUXNET2015 dataset was used.

2.4. Assessing the relationship between mWUE and IWUE

As a first step to conceptually understand the relationship between mWUE and IWUE, the relationship between IWUE and VPD was modeled by three hypothetical functions – linear, quadratic, and the Michaelis-Menten functions – based on the observations across the sites. The quadratic model of IWUE-VPD (hereafter $IWUE_Q$) depicts the case where IWUE increases with VPD until it reaches a maximum and then decreases afterward. In other words, when VPD is low, increasing IWUE with increasing VPD reflects a faster decrease of g_s than A (due to the high intercellular CO_2 concentration, c_i) while decreasing IWUE with increasing VPD at high

VPD reflects a faster decrease of A than g_s (low g_s at high VPD reduces c_i and eventually causes the steep decline of A). The linear model (hereafter $IWUE_L$), on the other hand, represents a simplified IWUE-VPD relationship where IWUE would keep increasing with rising VPD assuming IWUE is only limited by g_s but not by photosynthetic capacity. The Michaelis-Menten function (hereafter $IWUE_M$) represents the saturating IWUE under high VPD but does not account for IWUE reduction. Thus, the linear and quadratic functions are considered plausible "end-members" describing the actual response of IWUE to VPD, while the Michaelis-Menten function is a more intermediate case. Mathematically, the $IWUE_L$, $IWUE_M$, and $IWUE_Q$ take the forms:

$$IWUE_L = m\,VPD + n \qquad (9)$$

$$IWUE_M = \frac{IWUE_{max} \cdot VPD}{k + VPD} \qquad (10)$$

$$IWUE_Q = -a\,(VPD - b)^2 + c \qquad (11)$$

where m is the slope of $IWUE_L$, n is $IWUE_L$ at VPD = 0, $IWUE_{max}$ is the maximum potential IWUE, k is the VPD at which IWUE proceeds at half $IWUE_{max}$, a represents the curvature of $IWUE_Q$, b is the vertex, c is the maximum $IWUE_Q$ at the vertex.

The expected dynamics of mWUE across the FLUXNET sites in response to changing VPD were simulated based on an empirically driven IWUE-VPD model to understand how the mWUE metrics would respond to changing VPD and IWUE. To generate possible patterns of mWUE-VPD, the range of coefficients in the IWUE models was determined empirically from the data across the sites. To facilitate interpretation, the patterns were simulated by changing the curvature of the quadratic equation (Eq. 11), assuming the intercept is equal to zero. For the simulation of mWUE, a constant c_a was applied by calculating its average across the sites to focus on the interactions among VPD, IWUE, and mWUE (Eqs. 3 & 5).

Lastly, we investigated how IWUE (as a biological factor) and aridity index (as an environmental driver) influence the variability of mWUE. Based on the Eqs. 3 and 5, we hypothesized that a simple relationship between mWUE and the inverse of IWUE ($IWUE^{-1}$) might emerge and would be affected by changing moisture conditions. Therefore, we identified a relationship between mWUE and $IWUE^{-1}$ for each study site and examined whether the relationship can be generalized across the sites based on the site-specific aridity index.

3. Results

3.1. Empirical response of IWUE to changing VPD or AI

To test the robustness of IWUE as a proxy of intrinsic water-use efficiency at the ecosystem level, we first compared the two different definitions of intrinsic water-use efficiencies at stand level, GPP divided by surface conductance (G_s) (i.e., $iWUE = GPP/G_s$) and inherent WUE (i.e., $IWUE = GPP/ET \times VPD/P_a$). The two WUE definitions were linearly correlated across the study sites (Fig. 1), and most sites had coefficients of determination larger than 0.95 (Fig. 1b), suggesting the robustness of IWUE as a proxy of intrinsic water-use efficiency at the ecosystem level (see the Supporting Information for an additional comparison of multiple definitions of intrinsic water-use efficiency; Figs. S1 & S2). We also performed the entire analysis using these two WUE definitions and observed similar results, which led to the same conclusion. Therefore, we only show the results from using IWUE hereafter.

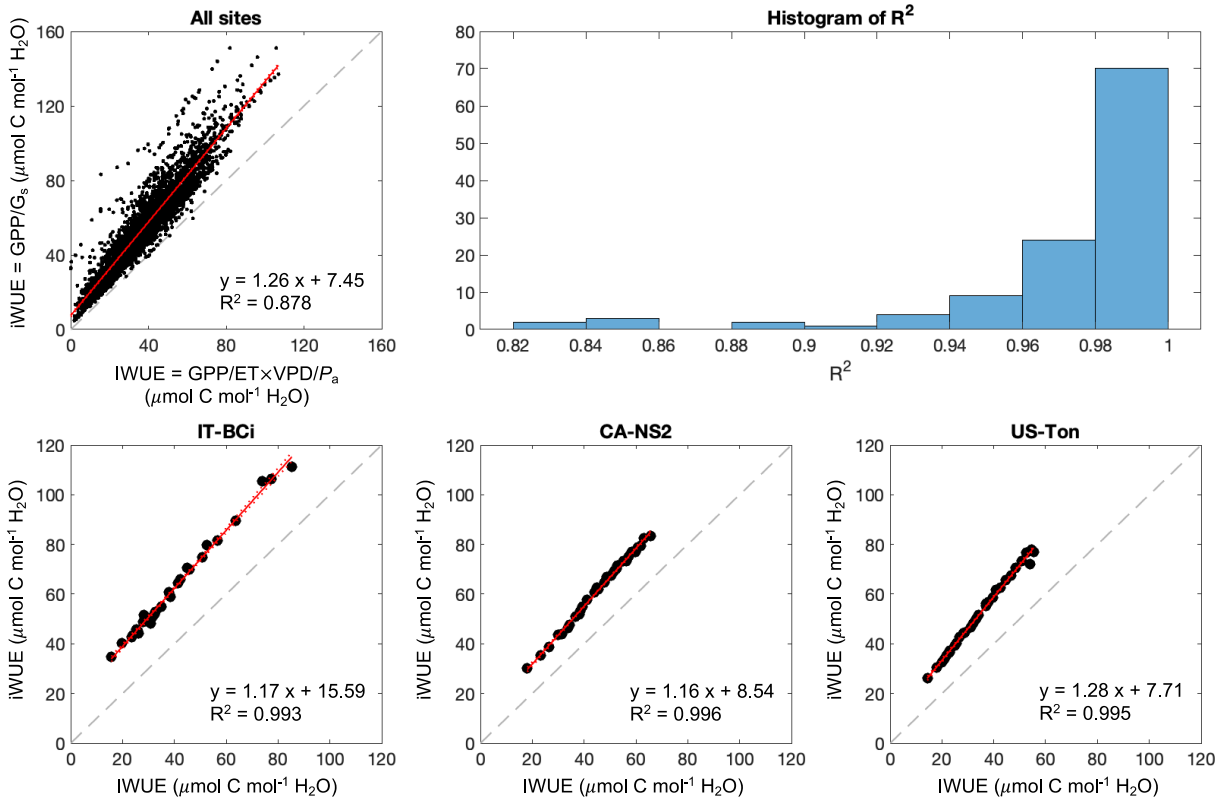

346

347 **Figure 1.** Comparison of two different definitions of water-use efficiencies at all sites (a) and at
348 three sample sites (c, d, e): inherent water-use efficiency at the ecosystem level, IWUE (=
349 GPP/ET×VPD/P_a), and intrinsic water-use efficiency at the ecosystem level, iWUE (= GPP/G_s).
350 Refer to Beer et al. (2009) for the comparison of different definitions of water-use efficiencies at
351 leaf and ecosystem-level. Individual dots in panels a, c, d, and e indicate WUE partitioned into
352 discrete bins spanning a range of VPD. Solid red lines indicate significant linear regressions ($P <$
353 0.05), and dashed red lines indicate 95% confidence interval. Dashed gray lines represent 1:1
354 lines. Panel b shows the histogram of coefficients of determination (R^2) of the linear fits between
355 IWUE and iWUE across the study sites.

356

357 In most cases, the Michaelis-Menten model and the quadratic model explained empirical
358 IWUE patterns across the range of VPD better than the linear model (Fig. 2 and Fig. S3 in the

Supporting Information). Specifically, the Michaelis-Menten model worked better for the sites where the increase of IWUE plateaued at high VPD, and the quadratic model worked better for the sites where IWUE started decreasing at very high VPD. On the other hand, the linear model often overestimated IWUE at low and high VPD, except the sites where IWUE-VPD was highly linear.

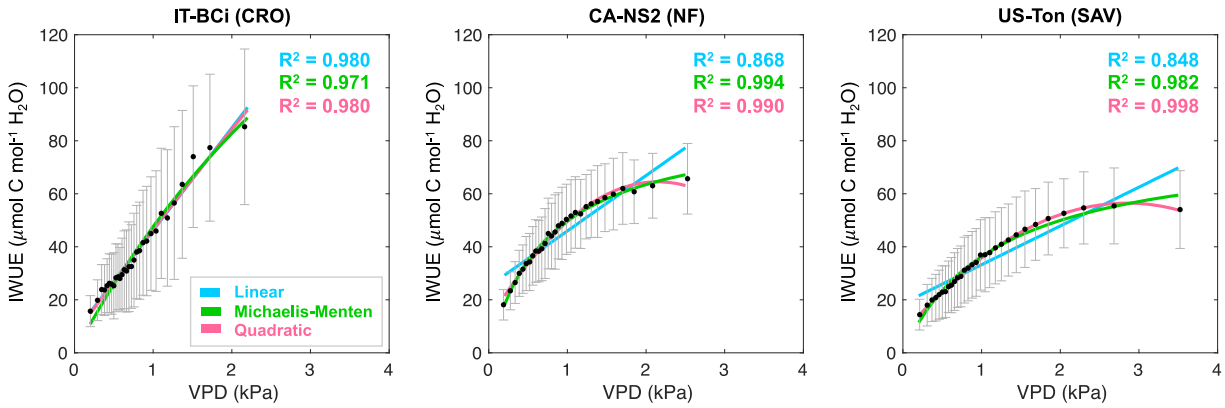

Figure 2. Examples of empirical (black dots) and modeled (linear: blue, Michaelis-Menten: green, quadratic: red) responses of inherent water-use efficiency (IWUE) to changing vapor pressure deficit (VPD). The examples include three sites best represented by the linear model (IT-BCi, cropland), the Michaelis-Mentes function (CA-NS2, needleleaf forest), and the quadratic model (US-Ton, savannah), respectively. Each error bar (light gray) represents the standard deviation of IWUE for each VPD bin (95% confidence). See Fig. S4 in the Supporting Information for the IWUE-VPD relationships of all the study sites (n = 115).

When the site-specific IWUE-VPD slope values derived from the linear model (i.e., m in Eq. 9) were combined, we found increasing m with rising aridity index ($P < 0.001$, Fig. 3a). However, site-level aridity did not influence the intercept of IWUE-VPD relationship ($P > 0.05$,

not shown here). When the sites were divided by their vegetation types, *m* increased with a rising aridity index in all vegetation types. However, the trend was only significant in grasslands, croplands, and shrublands ($P < 0.05$, Fig. 3).

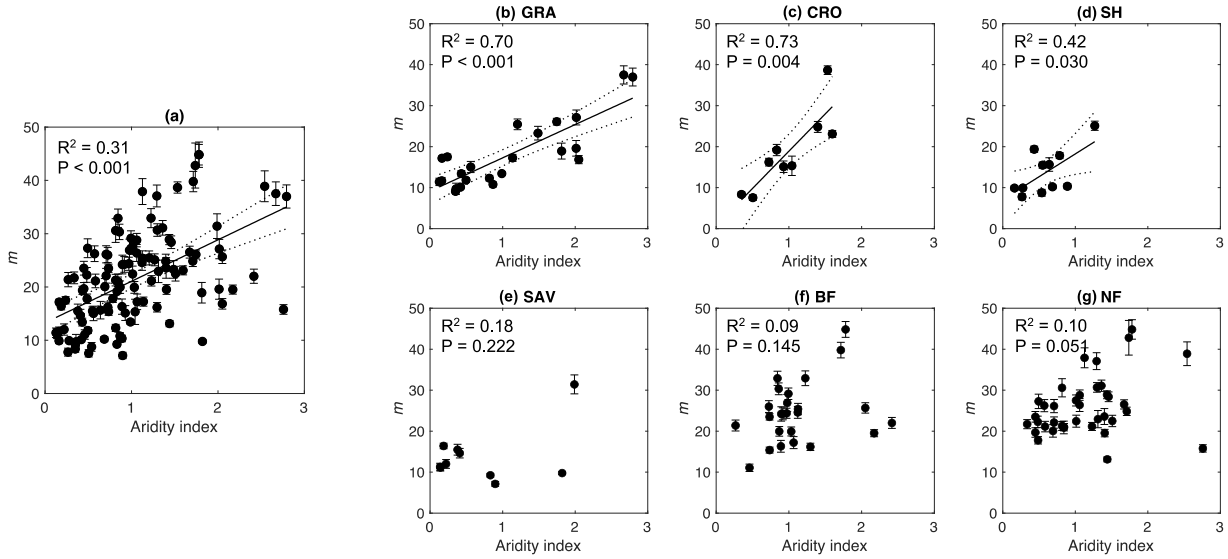

Figure 3. Relationship between the site-level aridity index and the regression slope of IWUE-VPD from individual sites (i.e., *m* in Eq. 9). Panel a shows the relationship when all sites were consolidated. The relationship is also illustrated separately for six different vegetation types in panels b to g. Each circle represents *m* from an individual site. Error bars represent standard errors of linear regressions. Solid lines indicate significant linear relationships ($P < 0.05$) and dashed lines indicate 95% confidence intervals.

3.2. Response of mWUE to changing VPD

Both of the mWUE indices, $\partial E/\partial A$ and squared g_1 (g_1^2), showed a very similar response to changing VPD and suggested that the directional change of mWUE can be interpreted differently depending on the pattern of IWUE-VPD (Fig. 4). When the iWUE-VPD relationship

is strongly linear, mWUE decreased exponentially and became less variable as VPD increased (Brighter curves in Figs. 4b & 4c). However, as the iWUE-VPD relationship became more non-linear, mWUE declined at lower VPD and then increased at higher VPD (i.e., concave-up), rendering the mWUE-VPD relationship non-monotonic (Darker curves in Figs. 4b & 4c).

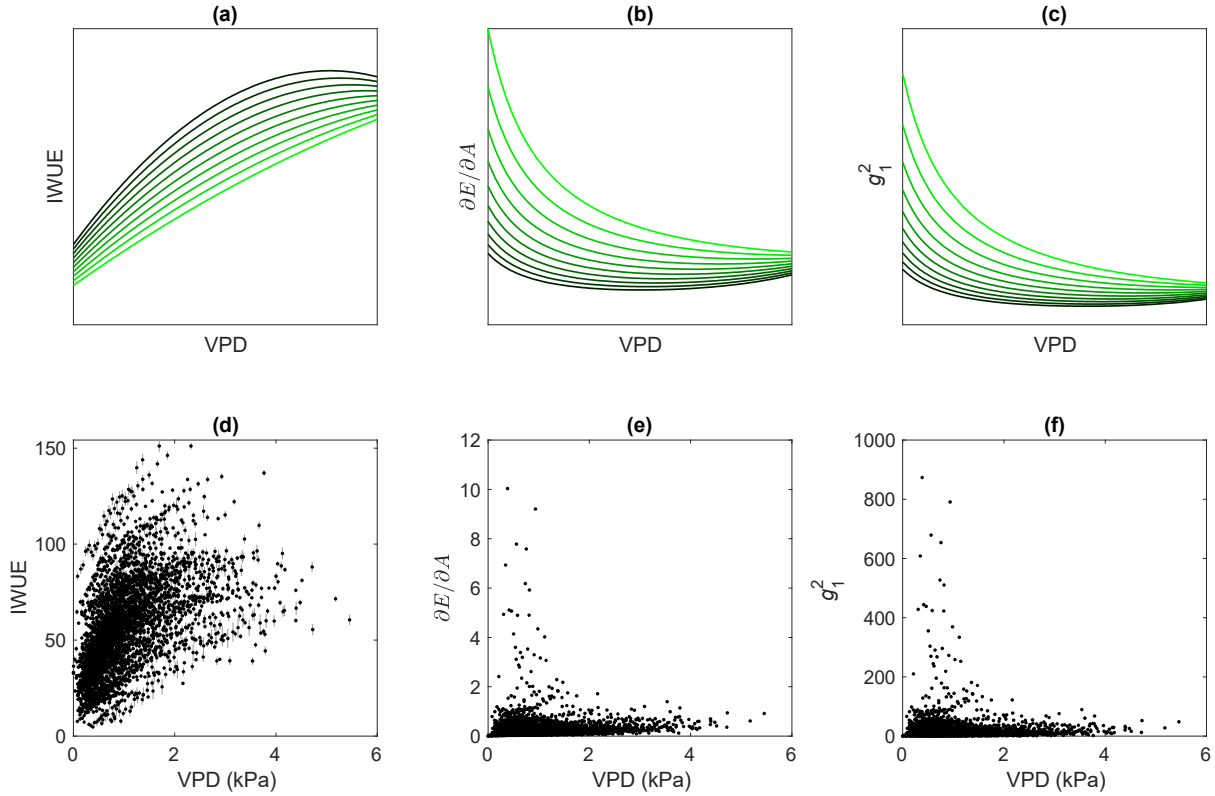

Figure 4. Hypothetical models of IWUE-VPD relationship (a), simulated $\partial E/\partial A$-VPD (b) and g_1^2-VPD (c) relationships based on typical cases, and their corresponding patterns illustrated using observations from all study sites (d, e, and f). The mWUE curves are the results of using the IWUE-VPD relationships of the corresponding colors. Note that IWUE-VPD relationships become more linear with lighter colors.

405 The simulated patterns of mWUE-VPD agreed well with the patterns from the empirical
406 observation when the appropriate function for the IWUE-VPD relationship was applied. We
407 show mWUE-VPD relationships from three study sites as examples (Fig. 5), of which IWUE-
408 VPD was represented best by linear, the Michaelis-Menten, and quadratic functions, respectively
409 (see Fig. 2 for their corresponding IWUE-VPD relationships. Also, see Fig. S5 in the Supporting
410 Information for the results of all study sites). As suggested by the simulation, the site with highly
411 linear IWUE-VPD (IT-BCi) showed exponentially decreasing mWUE with rising VPD. In
412 contrast, the other two sites with highly non-linear IWUE-VPD relationships had a concave-up
413 pattern of mWUE-VPD. Notably, the mWUE-VPD relationship generated using a less optimal
414 IWUE-VPD model can differ substantially from the empirical pattern. For example, application
415 of linear IWUE-VPD function to the CA-NS2 and US-Ton, the sites represented best by the
416 Michaelis-Menten and quadratic functions, respectively, generated concave-down mWUE-VPD
417 pattern that is opposite to the actual pattern (Fig. 5). The disagreements between models and
418 observations increased as VPD approached very high and very low extremes.
419

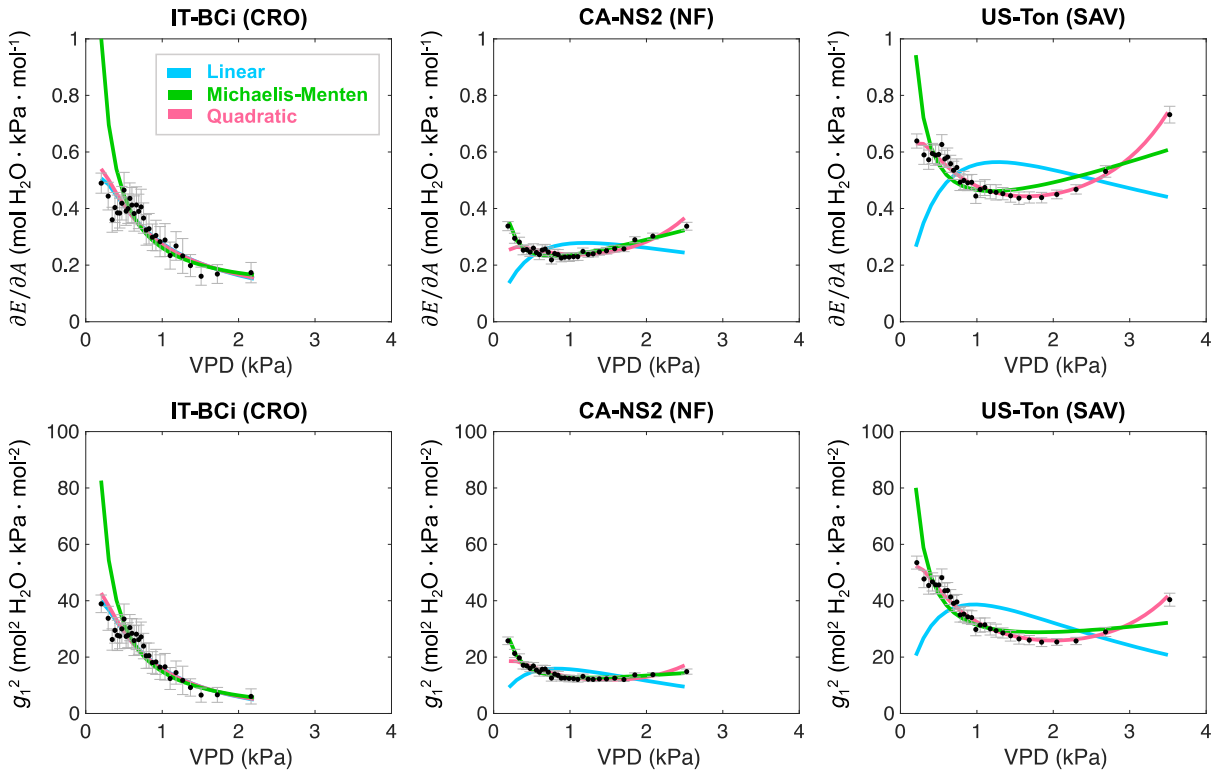

Figure 5. Examples of empirical (black dots) and modeled (linear: blue, Michaelis-Menten: green, quadratic: red) relationships between $\partial E/\partial A$ (analytical solution by Katul et al., 2010) and vapor pressure deficit (VPD), and between g_1^2 (Medlyn et al., 2012) and VPD. The examples include three sites best represented by the linear IWUE-VPD model (IT-BCi, cropland), the Michaelis-Menten function (CA-NS2, needleleaf forest), and the quadratic model (US-Ton, savannah), respectively. See Fig. 2 for the IWUE-VPD relationships at the corresponding sites. Each error bar (light gray) represents the standard error of the mean IWUE for each VPD bin (95% confidence). See Fig. S5 in the Supporting Information for the $\partial E/\partial A$ -VPD relationships at the 115 study sites.

The variability of mWUE to changing VPD was substantial in most cases (Fig. 6). Out of the total of 115 study sites, the percent increase of $\partial E/\partial A$ (i.e., growth in $\partial E/\partial A$ from the

lowest to the largest value at a site) was larger than 50% in 43 sites, and larger than 100% in 22 sites. Note that the reported percent increase was determined by excluding the upper and lower 10% of values. This step was taken to prevent exaggeration caused by extremely high $\partial E/\partial A$ at low VPD, which is commonly observed across the study sites (see Figure S5 in the Supporting Information for the variability of $\partial E/\partial A$ with VPD at all the study sites). As a result, the reported percent increase represents a conservative estimate overall.

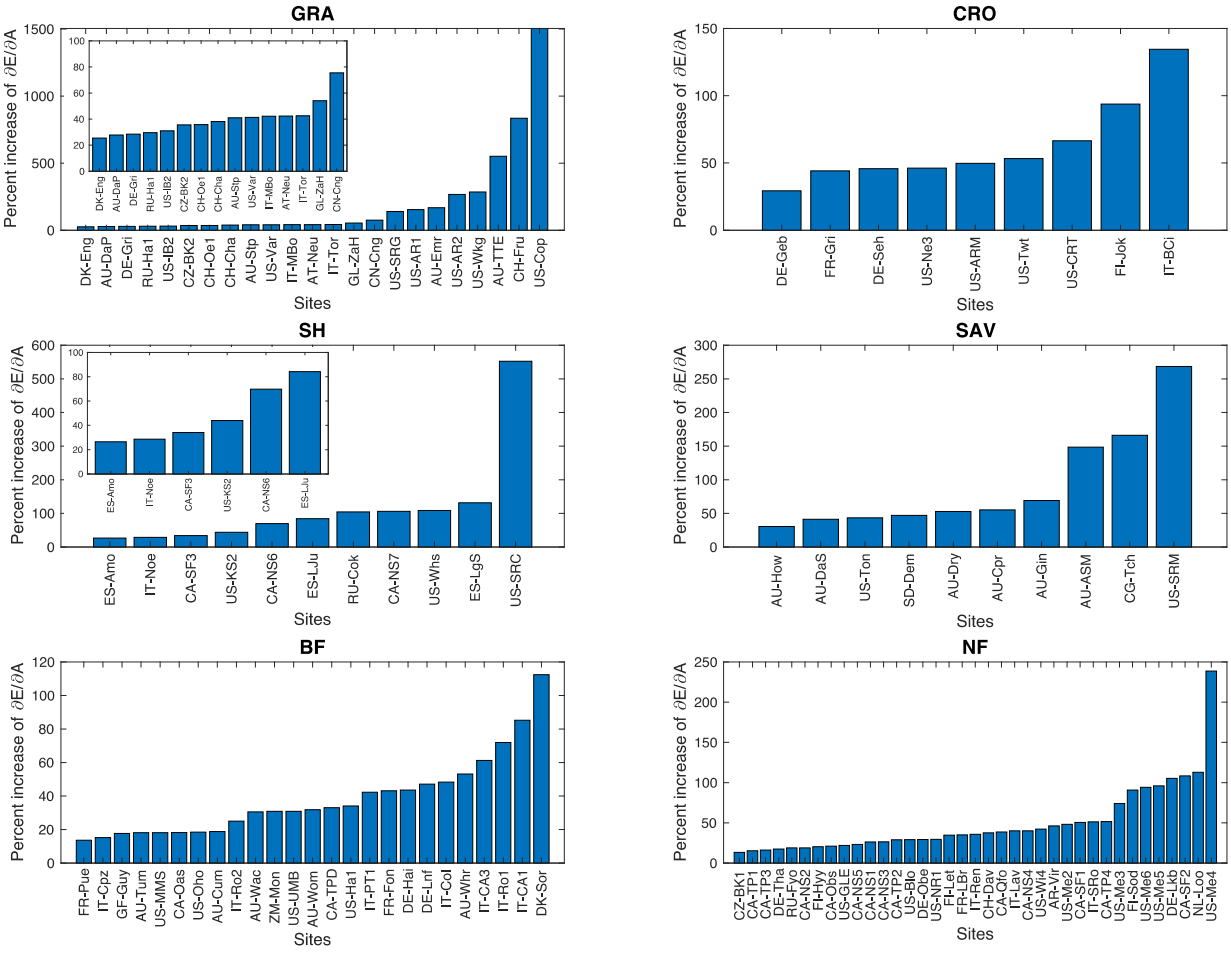

Figure 6. Sorted percent increase of $\partial E/\partial A$ (from the lowest $\partial E/\partial A$). Embedded plots in GRA and SH are zoomed in for those sites where percent increases are lower than 100%. Note that the percent increases were calculated after removing values of the highest 10% and lowest 10% to avoid exaggeration due to very high $\partial E/\partial A$ at low VPD at some sites. Therefore, the reported percent increase values are conservative estimates for most sites.

3.3. Correlation between mWUE and IWUE

Although the trend of mWUE-VPD seems hard to generalize, the simulated mWUE had a clear linear relationship with $IWUE^{-1}$ for the majority of IWUE's range regardless of the linearity of the IWUE-VPD relationship except when IWUE is very high (i.e., under high VPD, Fig. 7). While it is limited to a small portion of the entire range, there was a sharp directional change in the variation of mWUE near a point where $IWUE^{-1}$ was smallest, and strong linearities between mWUE and $IWUE^{-1}$ were found before and after the transitional point. Substantial hysteresis became more evident as the IWUE-VPD pattern became more curved (darker curves in Fig. 4).

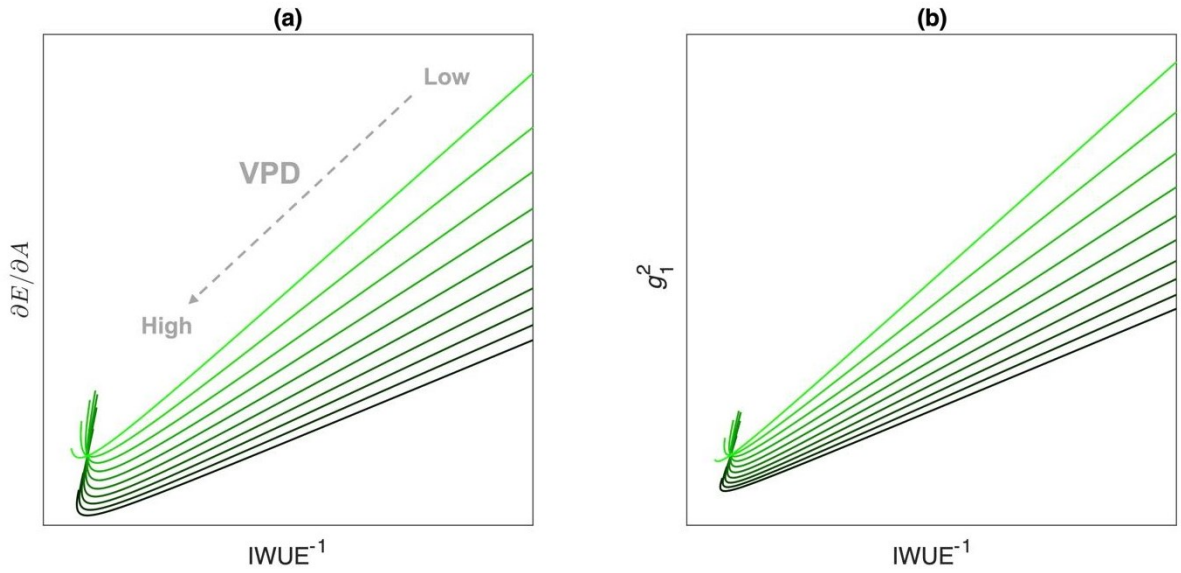

Figure 7. Simulated relationship between mWUE and $IWUE^{-1}$ (based on the hypothetical IWUE-VPD model in Fig. 4). The colors of the curves correspond to those used in Fig. 4: IWUE-VPD relationships become more linear with lighter colors. Dashed arrows in panel a represent the directional change of VPD from low to high VPD.

As predicted by the simulated mWUE-$IWUE^{-1}$ relationships (Fig. 7), the empirical mWUE-$IWUE^{-1}$ relationship was strongly linear ($P < 0.001$ at all sites, Fig. 8). A sign of hysteresis was noticeable for the site that showed decreasing iWUE under very high VPD (US-Ton, see Fig. 2 for its IWUE-VPD relationship). In contrast, hysteresis was less evident at the other sites. When the relationship was drawn by grouping data by different levels of IWUE (black dots in Fig. 8), hysteresis was not observed, and the mWUE-$IWUE^{-1}$ relationship was strongly linear.

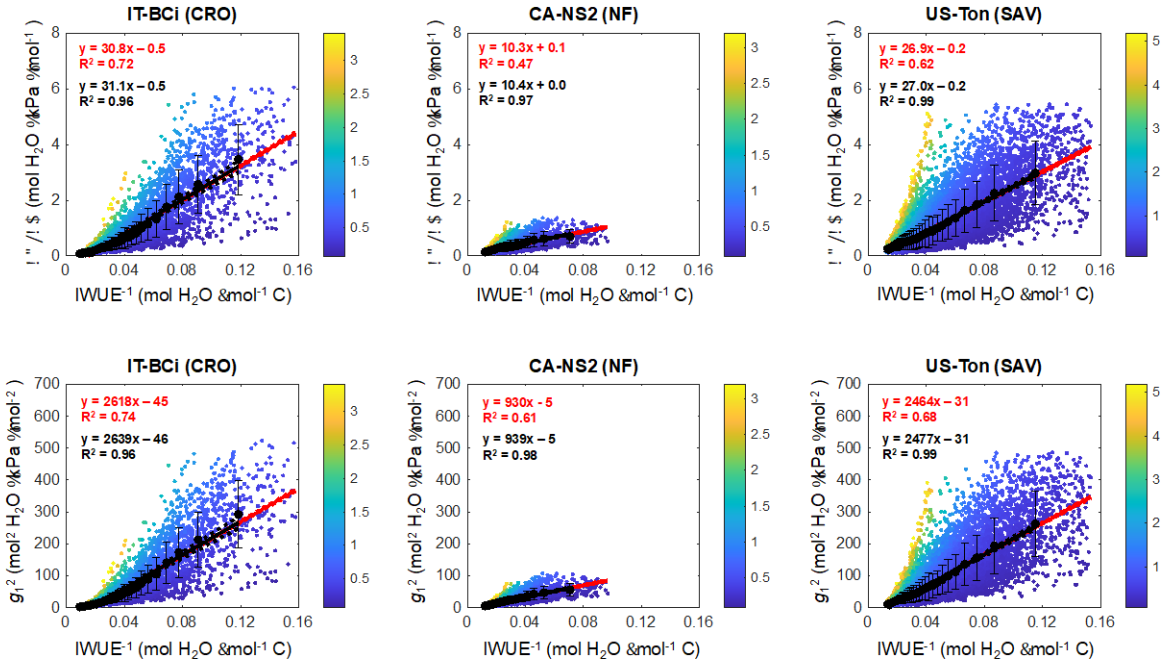

Figure 8. Examples of empirical relationship between mWUE and $IWUE^{-1}$. The examples include three sites best represented by the linear IWUE-VPD model (IT-BCi, cropland), the Michaelis-Mentes function (CA-NS2, needleleaf forest), and the quadratic model (US-Ton, savannah), respectively. See Fig. 2 for the IWUE-VPD relationships at the corresponding sites. Colorful dots represent hourly data points shaded based on the level of VPD (see color bars for the scale of VPD). Black dots represent data binned by $IWUE^{-1}$: Data binning was performed to distribute sample sizes evenly across bins (~30 samples per bin). Error bars represent standard deviations. The red and black solid lines indicate linear fits for hourly and binned data, respectively. Dashed red lines represent confidence intervals for the slopes of linear regressions. Note that red and black linear regressions and their confidence intervals overlap. See Fig. S6 in the Supporting Information for the $\partial E/\partial A$ - $IWUE^{-1}$ relationships at the 115 study sites.

We investigated whether the relationship between mWUE and $IWUE^{-1}$ could be generalized across the sites based on the site-specific AI. Specifically, the linear $IWUE^{-1}$ – mWUE slopes (hereafter m^*) from all study sites were merged, and their variability in response to changing AI was evaluated. We found a significant linear relationship between m^* and AI when both are scaled by $\log_{10}$ ($P < 0.001$, Fig. 9). The m^* was larger at the drier sites (i.e., sites of lower AI) than at the wetter sites (i.e., sites of larger AI). However, we did not find a significant relationship between the $IWUE^{-1}$ – mWUE intercept and AI ($P > 0.05$, not shown here).

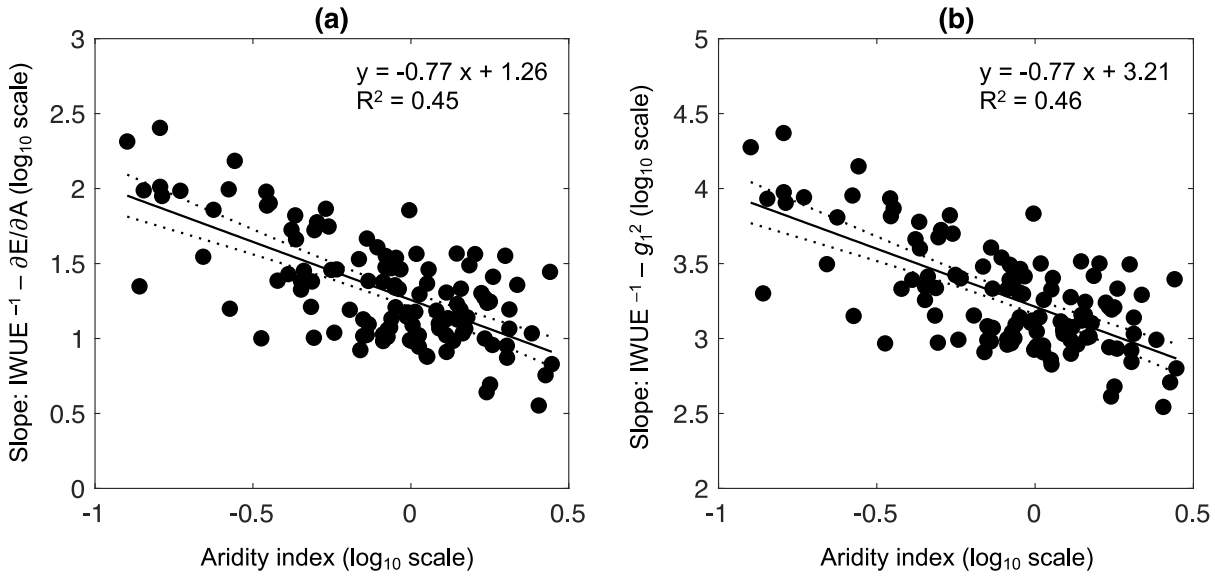

492

493 **Figure 9.** Relationships between IWUE^{-1}-mWUE slope and aridity index (= P/PET) derived
494 from all the study sites (n = 115). Each circle represents the slope obtained from an individual
495 site. Both the x and y axes are scaled by $\log_{10}$. Solid red lines indicate linear regressions and
496 dashed lines indicate confidence intervals (95% confidence interval).

497

498 We further tested whether we could find the similar relationship when the sites were grouped by
499 the vegetation type. We found decreasing m^* with rising AI in grasslands, croplands, and
500 shrublands ($P < 0.01$, Fig. 10). On the other hand, m^* was relatively constant across the range of
501 AI in savannas, deciduous broadleaf forests, and evergreen needleleaf forests ($P > 0.05$, Fig. 10).

502

503

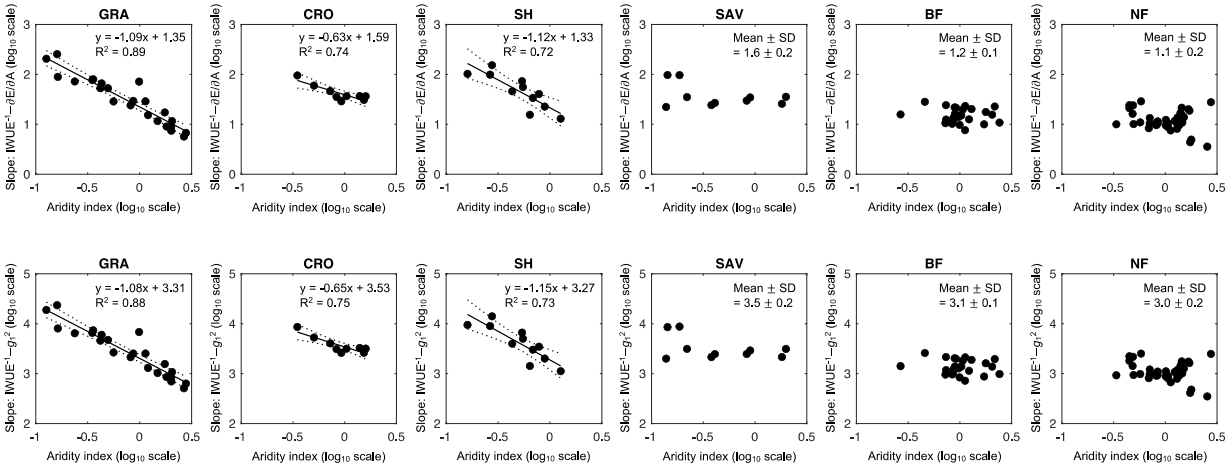

Figure 10. Relationships between log-transformed $IWUE^{-1}$-mWUE slope and aridity index in different vegetation types (GRA: grassland, CRO: cropland, SH: shrubland, SAV: savanna, BF: broadleaf forest, NF: needleleaf forest). Each circle represents the log-transformed slope obtained from an individual site. Solid lines indicate significant linear relationships ($P < 0.05$) and dashed lines indicate 95% confidence intervals.

4. Discussion

Stomatal optimization theory, which originated with the work of Cowan and Farquhar (1977), has experienced a recent surge in popularity as the vegetation modeling community continually seeks ways to inject more theoretical rigor into Earth system models (Anderegg et al., 2018; Bassiouni & Vico, 2021; Bonan et al., 2014; Feng et al., 2022; Katul et al., 2010; Katul et al., 2009; Lin et al., 2018; Lin et al., 2015; Lu et al., 2020; Lu et al., 2016; Medlyn et al., 2012, 2017; Novick et al., 2016b; Sabot et al., 2022; Sperry et al., 2017; Wolf et al., 2016). The marginal water-use efficiency (mWUE) is a key parameter in this type of model, but we still need a clear understanding of how mWUE is regulated biologically and environmentally. Lin et al. (2018) previously suggested suboptimal mWUE in response to VPD at a sub-daily scale by

estimating site-specific, best-fitted exponent for VPD based on the variation model of optimality theory (Medlyn model), which inspired our study. In comparison, our study is unique in analyzing the dynamics of mWUE observed at the hourly timescale in response to changing VPD owing to the long-term continuous carbon and water flux data from the network of eddy covariance towers.

Another motivation for our study was the conflicting arguments over the dynamics of mWUE in response to water stress. While mWUE is in general considered to be nearly constant during a day under stable soil moisture conditions (Berninger & Hari, 1993; Fites & Teskey, 1988; Hall & Schulze, 1980; Hari et al., 2000), several studies showed that mWUE changed with different levels of water stress. For example, theoretical considerations suggest a monotonic decrease of mWUE with higher water stress when the stochasticity of rainfall depths is neglected (Cowan, 1982; Makela et al., 1996), while some empirical estimates showed that mWUE increases under severe water stress (Farquhar et al., 1980b; Grieu et al., 1988). On the other hand, Manzoni et al. (2011) performed a meta-analysis of 50 species to estimate mWUE from gas exchange observations along gradients of soil moisture and showed that mWUE decreases under mild water stress but increases under severe water stress (note that they defined $\lambda = \partial A/\partial E$, which is inverse of the definition used by Cowan & Farquhar (1977) and this study).

4.1. Relationship between IWUE and VPD

Based on the two equations of stomatal optimization theory (Eqs. 3 & 5), we first characterized the variability of mWUE based on the relationship between IWUE and VPD, representing biological and environmental factors, respectively. We show that the variability of IWUE must be modeled accurately to emulate the variability of mWUE in response to water

544 stress correctly. For example, as demonstrated in Fig. 5 (CA-NS2 & US-Ton), oversimplifying
545 the IWUE-VPD relationship by modeling it with a linear function can incorrectly interpret
546 mWUE variability.

547 The non-linear IWUE-VPD relationship is presumably driven by different rates of carbon
548 assimilation and water loss in response to changing VPD at an hourly scale, reflecting the
549 balance between stomatal and non-stomatal limitations to photosynthesis at the leaf level
550 (Farquhar, 1978; Jones, 2014). Under low to moderate VPD conditions, photosynthesis is less
551 sensitive to changing intercellular CO_2 concentration because stomatal conductance is high
552 enough to maintain the high intercellular CO_2 when VPD is low to moderate. Therefore, the
553 quantity of reduced water loss by stomatal closure (ET at an ecosystem level) outweighs the
554 quantity of reduced carbon assimilation (GPP at an ecosystem level*)* when VPD rises (i.e.,
555 $|\Delta GPP| < |\Delta ET|$), resulting in the increasing phase of IWUE. As VPD keeps increasing,
556 photosynthesis can be limited when the reduction of stomatal conductance under high VPD
557 conditions substantially reduces intercellular CO_2 concentration (i.e., $|\Delta GPP| \approx |\Delta ET|$),
558 resulting in the steady phase of IWUE. As VPD becomes excessively high, photosynthesis will
559 be further suppressed by high temperature (Yamori et al., 2014) and low leaf water potential
560 (Lawlor & Tezara, 2009) that are associated with dry conditions (i.e., $|\Delta A| > |\Delta g_s|$), leading to
561 the decreasing phase of IWUE.

562 Therefore, assuming a linear IWUE-VPD relationship may not only fail to emulate
563 observations but also oversimplify the physiological responses to water stress. Our analysis
564 recommends employing the Michaelis-Menten function for most sites while utilizing a quadratic
565 function for sites exhibiting extreme cases where IWUE declines under high VPD conditions.
566 The Michaelis-Menten function can be beneficial to characterize the IWUE-VPD relationship

since the maximum potential IWUE and the rate of IWUE increase can be identified during parameterization (Eq. 10). While the quadratic function can emulate IWUE-VPD relationships very well or performs even better than the Michaelis-Menten function in some cases where IWUE decreases at high VPD, it is parameterized empirically and as a result, lacks mechanistic information. Nevertheless, the quadratic function is preferable to the linear function.

It is also important to consider the definition of water-use efficiency for accuracy. We used inherent water-use efficiency (IWUE) as a proxy of intrinsic water-use efficiency (iWUE) at the ecosystem level as suggested by Beer et al. (2009), which can be estimated by GPP and ET inferred from the flux tower observations. This approximation is particularly useful over a more common ecosystem-level iWUE = GPP/G_s because IWUE requires fewer variables and is easier to extrapolate to a larger scale. However, it is important to note that ET/VPD in the equation of IWUE (Eq. 6) is a proxy of canopy conductance, assuming the canopy is well coupled to the atmosphere, boundary layer resistance is small, and thermal equilibrium between leaf and air is achieved (Beer et al., 2009). In other words, IWUE under non-equilibrium between canopies and atmosphere can be overestimated due to the higher VPD than the vapor pressure gradient near the canopy surface (i.e., the difference between intercellular vapor pressure (e_i) and atmospheric vapor pressure (e_a), $e_i - e_a$). Difference between leaf and air temperature can also influence the $e_i - e_a$; if leaf temperature is higher than air temperature (as it often is, e.g., Novick & Barnes, 2023; Yi et al., 2020), e_i will increase while e_a remains constant, resulting in larger $e_i - e_a$ than measured VPD and consequently underestimate IWUE. Therefore, it is important to address this potential bias to quantify iWUE accurately. According to our results, there was a strong correlation between the two ecosystem-level iWUE proxies at the site level (Fig. 1), implying that the choice of ecosystem-level iWUE definition is unlikely to influence our interpretation of

590 the iWUE and mWUE variabilities substantially. Furthermore, our comparison of multiple
591 definitions of iWUE using a mechanistic model, CANVEG (see the Supporting Information for
592 more details), suggested that IWUE is a good proxy of leaf-level iWUE and meets the general
593 assumptions to address scaling issues. Thus, we conclude that eddy covariance observation of
594 carbon and water fluxes is suitable to model the variability of intrinsic water-use efficiency in
595 response to changing VPD.

596 It is worth mentioning that there was a stronger linear relationship between the slope of
597 IWUE-VPD and aridity index (Fig. 4) in the ecosystems characterized by lower vegetation types
598 (e.g., grasslands, croplands, and shrubland). In contrast, ecosystems with higher vegetation (e.g.,
599 savannahs, broadleaf forests, and needleleaf forests) exhibited a weaker relationship. This
600 observation implies a potential link between water-use efficiency and the vertical structure of
601 vegetation, although the exact underlying mechanism remains uncertain.

602

603 **4.2. Modeling the variability of mWUE**

604 We compared two solutions of mWUE by Katul et al. (2010) ($\partial E/\partial A$) and Medlyn et al.
605 (2012) (g_1) developed based on different assumptions on stomatal optimality (carbon-limited vs.
606 light-limited) for more robust conclusion. Despite the difference in the assumption, both
607 solutions yielded very similar results throughout our analysis, confirming that the optimality
608 assumption had little impact on evaluating the variability of mWUE in response to changing
609 moisture conditions.

610 We characterized the trend of mWUE by using VPD as an environmental driver (Figs. 4
611 & 5), where its variability in response to VPD was unique and not necessarily unidirectional,
612 thus making it hard to generalize with commonly available functions. Specifically, the variability

of mWUE was simpler and decreased exponentially with rising VPD when the IWUE-VPD relationship was more linear, making it easy to model the mWUE-VPD relationship (Figs. 4 & 5). However, the variability of mWUE was not unidirectional when the IWUE-VPD relationship was non-linear, as observed in most cases (Fig. S5 in the Supporting Information); high variability in mWUE is usually observed at low- and high-ends of VPD. On the other hand, when mWUE was calculated under conditions of moderate VPD level only, the variability of mWUE can be overlooked and considered constant. This complex pattern signifies the importance of a comprehensive view of IWUE and mWUE across the full potential range of VPD. Observation under conditions of a partial range of environmental factors is common in many types of field measurements that have coarser time resolution (hourly vs. daily to weekly, e.g., eddy covariance vs. leaf gas exchange measurements) unless they are performed frequently over a long period to cover non-typical conditions. We were able to estimate precise variability of mWUE matching with the hypothetical models owing to the large amount of data (FLUXNET2015) collected every half-hour over the long period throughout the network of flux towers (total 1,036 site years with many sites offering data collected over more than a decade), highlighting the value of long-term, continuous measurements. Overall, our result of the mWUE-VPD relationship supports the results of Manzoni et al. (2011) among the various conflicting results over the response of mWUE in response to water stress, which found decreasing mWUE under mild water stress and increasing mWUE under severe water stress from a meta-analysis of gas exchange observations.

As a solution to model unique patterns of mWUE, we attempt to address its variability with information that can be obtained easily from various types of field measurements (e.g., eddy covariance, gas exchange, and tree-ring cores) and modeled empirically – IWUE. The relationship between mWUE and IWUE was inferred from the two equations of the optimization

theory (Eqs. 3 & 5). We found a strong linear correlation between $IWUE^{-1}$ and mWUE from both empirical data (Fig. 8) and modeling exercise (Fig. 7). In other words, the variability of mWUE in response to changing VPD can be characterized by 1) the function of IWUE-VPD relationship and 2) the slope between $IWUE^{-1}$ and mWUE. The relationship between IWUE-VPD is relatively simple and can be identified with various field measurements. This raises the question of whether a simple way exists to identify the slope between $IWUE^{-1}$ and mWUE. By synthesizing the $IWUE^{-1}$-mWUE slopes across the sites, we found that the IWUE-mWUE slope is highly correlated with the site-specific aridity index that can be characterized for different vegetation types (Fig. 9). The correlation is conceivable from the equations of mWUE (Eqs. 3 & 5). If, for instance, Eq. 3 is rearranged,

$$\frac{\partial E/\partial A}{IWUE^{-2}} \propto VPD \qquad (12)$$

indicating that the slope between mWUE and the inverse of IWUE is proportional to VPD, which is commensurate with aridity index at a site-level. The correlation between the $IWUE^{-1}$-mWUE slope and the aridity index at a site level implies that the aridity index is a good surrogate for the site-specific $IWUE^{-1}$-mWUE slope.

We further illustrated how the correlations between the $IWUE^{-1}$-mWUE slope (m^*) and aridity index (AI) vary across vegetation types (Fig. 10). Among the vegetation types, GRA, CRO, and SH had strong correlations between m^* and AI, which suggested using different m^* depending on the site-level dryness. On the other hand, the low variability of m^* observed in SAV, BF, and NF suggests that constant m^* can generate a reasonably accurate mWUE-VPD relationship regardless of the site-level dryness. Although the reasons for this difference are not entirely clear, this empirical relationship will help more accurately model the variability of mWUE in response to changing VPD across the sites and biomes. Growth in data availability

659 across the flux tower network will ensure the coverage of the full potential range of
660 environmental factors. More data availability can be achieved by consistently collecting good-
661 quality data from existing study sites and establishing new sites in underrepresented areas.
662 Furthermore, it will also help the development of $m*$ in detail, for instance, based on the plant
663 water-use strategies, with the aid of conjoined field measurements such as water potential (Ψ) of
664 soil and plant.
665
666 **4.3. Implications for future research**
667 It is important to note that plant response to water stress is not only determined by the
668 water demand (i.e., atmospheric dryness or VPD) but also by the availability of water sources
669 (i.e., soil moisture). While volumetric soil moisture content (θ) is often considered as a metric of
670 soil water available to plants, soil water potential (Ψ_S) is the driving force of water flows that
671 becomes available to plants by moving along gradients of water potential through the plant (stem
672 and leaf) and eventually to the air. Moreover, Ψ_S is not only determined by the θ but also by soil
673 physical properties, and thus can differ even under conditions of the same θ (Campbell, 1974;
674 van Genuchten, 1980). Unlike Ψ_S, θ is widely measured and usually available with flux data, and
675 carbon and water fluxes are often explained as a function of θ (Green et al., 2019; Novick et al.,
676 2016a). However, θ may not characterize soil moisture availability to plants properly, and its
677 relationship with carbon and water fluxes is usually nonlinear and threshold-driven (Feldman et
678 al., 2019; Novick et al., 2022; Stocker et al., 2018), making the modeling of the relationship
679 between IWUE and soil moisture availability challenging. Therefore, enhanced accessibility to
680 Ψ_S data by improving the ease and reliability of Ψ_S observations, for example, by building a
681 centralized and standardized network of Ψ (Novick et al., 2022) will be a necessary step to better

characterize the impact of soil moisture availability on plant responses such as IWUE and mWUE.

In this study, we tested the two stomatal optimization models (Katul et al., 2010; Medlyn et al., 2012) that are elaborations of the original Cowan & Farquhar model (1977) with little modifications because our goal was to characterize variability of mWUE in response to dryness (VPD and aridity index) using IWUE that can be calculated from the extensive, long-term continuous data from the network of eddy covariance. Meanwhile, more recent optimization models are incorporating additional physiological penalties than the water loss, for instance, damage to the vascular system induced by water stress (Anderegg et al., 2018; Sperry et al., 2017; Wolf et al., 2016), which will enhance prediction of long-term plant responses to climate change. While monitoring the integrity of the vascular system, which can be informed by the dynamics of hydraulic conductivity, has not been widely conducted, recent advances in psychrometric approaches allowing continuous measurements of plant Ψ (e.g., PSY1 by ICT International) and Ψ_S (e.g., TEROS 21 by Meter Group) are now enabling the monitoring the dynamics of hydraulic conductivity. Moreover, the relationship between plant and soil Ψ can be used to identify plant water-use strategies (e.g., isohydry framework; Martinez-Vilalta et al., 2014), which will help develop m^* based on plant water-use strategies. The measurements of carbon and water fluxes using the eddy covariance technique with the aid of the centralized and standardized deployment of Ψ sensors (Novick et al., 2022) will have a great potential to test models and theories of stomatal optimization and advance our knowledge of it.

Acknowledgments

We thank FLUXNET/AmeriFlux community for managing their sites, collecting and processing data, and making data available to public and broader scientific community. K.Y. and G.B.S. acknowledge support from the NSF Division of Earth Sciences (Grant # 2012893) through CUAHSI and the USGS John Wesley Powell Center for Analysis and Synthesis. K.A.N and T.H. were supported by the NASA Carbon Science Program (Grant # NNX17AE69G). K.A.N. also acknowledges support from the NSF Division of Environmental Biology (Grant # 1552747), the NSF Division of Integrative Organismal Systems (Grant #2006196), and the AmeriFlux Management Project. L.W. was supported by the NSF Division of Earth Sciences (Grant # 1554894). X.Y. was supported by the NSF Division of Integrative Organismal Systems (Grant # 2005574). K.M. was supported by the INTER Mobility Fellowship from the FNR Luxembourg (INTER/MOBILITY/2020/14521920/MONASTIC). The findings and conclusions in this publication are those of the authors and should not be construed to represent any official USDA or U.S. Government determination or policy.

Author Contributions

K.Y., K.A.N., and D.B. conceptualized the research and developed the methodology. K.Y., D.B., and M.B. analyzed the data, and K.A.N, Q.Z., L.W., T.H., X.Y., K.M., and G.B.S. validated the analysis. K.Y. visualized the data analysis. K.Y. wrote the manuscript with input and revisions from all authors.

Conflict of Interest

The authors declare that they have no conflict of interest.

Data Availability

The data that support the findings of this study are openly available in the FLUXNET Data Portal at https://fluxnet.org/data/fluxnet2015-dataset/. The list of DOIs for the individual FLUXNET sites used in this study is available in the Supporting Information (Table S1).

References

Allen, R. G., Pereira, L. S., Raes, D., & Smith, M. (1998). Crop evapotranspiration-Guidelines for computing crop water requirements-FAO Irrigation and drainage paper 56. *FAO, Rome*, *300*(9), D05109.

Anderegg, W. R. L., Wolf, A., Arango-Velez, A., Choat, B., Chmura, D. J., Jansen, S., Kolb, T., Li, S., Meinzer, F. C., Pita, P., de Dios, V. R., Sperry, J. S., Wolfe, B. T., & Pacala, S. (2018). Woody plants optimise stomatal behaviour relative to hydraulic risk. *Ecology Letters, 21*(7), 968–977. https://doi.org/10.1111/ele.12962

Anderegg, W. R. L., Wolf, A., Arango-Velez, A., Choat, B., Chmura, D. J., Jansen, S., Kolb, T., Li, S., Meinzer, F., Pita, P., de Dios, V. R., Sperry, J. S., Wolfe, B. T., & Pacala, S. (2017). Plant water potential improves prediction of empirical stomatal models. *PLoS One*, *12*(10), e0185481. https://doi.org/10.1371/journal.pone.0185481

Baldocchi, D. D., & Harley, P. C. (1995). Scaling carbon dioxide and water vapour exchange from leaf to canopy in a deciduous forest. II. Model testing and application. *Plant, Cell & Environment*, *18*(10), 1157–1173. https://doi.org/10.1111/j.1365-3040.1995.tb00626.x

Baldocchi, D., & Meyers, T. (1998). On using eco-physiological, micrometeorological and biogeochemical theory to evaluate carbon dioxide, water vapor and trace gas fluxes over

749 vegetation: A perspective. *Agricultural and Forest Meteorology*, *90*(1), 1–25.
750 https://doi.org/10.1016/S0168-1923(97)00072-5
751 Baldocchi, D. D., Keeney, N., Rey-Sanchez, C., & Fisher, J. B. (2022). Atmospheric humidity
752 deficits tell us how soil moisture deficits down-regulate ecosystem evaporation. *Advances*
753 *in Water Resources*, *159*, 104100. https://doi.org/10.1016/j.advwatres.2021.104100
754 Ball, J. T., Woodrow, I. E., & Berry, J. A. (1987). A Model Predicting Stomatal Conductance
755 and its Contribution to the Control of Photosynthesis under Different Environmental
756 Conditions. In: Biggins, J. (Ed.), *Progress in Photosynthesis Research*. pp. 221–224.
757 Springer, Dordrecht. https://doi.org/10.1007/978-94-017-0519-6_48
758 Bassiouni, M., & Vico, G. (2021). Parsimony vs predictive and functional performance of three
759 stomatal optimization principles in a big-leaf framework. *New Phytologist*, *231*(2), 586–
760 600. https://doi.org/10.1111/nph.17392
761 Beer, C., Ciais, P., Reichstein, M., Baldocchi, D., Law, B. E., Papale, D., Soussana, J.-F.,
762 Ammann, C., Buchmann, N., Frank, D., Gianelle, D., Janssens, I. A., Knohl, A., Köstner,
763 B., Moors, E., Roupsard, O., Verbeeck, H., Vesala, T., Williams, C. A., & Wohlfahrt, G.
764 (2009). Temporal and among-site variability of inherent water use efficiency at the
765 ecosystem level. *Global Biogeochemical Cycles*, *23*(2).
766 https://doi.org/10.1029/2008GB003233
767 Beer, C., Reichstein, M., Tomelleri, E., Ciais, P., Jung, M., Carvalhais, N., Rodenbeck, C.,
768 Arain, M. A., Baldocchi, D., Bonan, G. B., Bondeau, A., Cescatti, A., Lasslop, G.,
769 Lindroth, A., Lomas, M., Luyssaert, S., Margolis, H., Oleson, K. W., Roupsard, O., …
770 Papale, D. (2010). Terrestrial gross carbon dioxide uptake: Global distribution and

771 covariation with climate. *Science*, *329*(5993), 834–838.
772 https://doi.org/10.1126/science.1184984
773 Béland, M., & Baldocchi, D. D. (2021). Vertical structure heterogeneity in broadleaf forests:
774 Effects on light interception and canopy photosynthesis. *Agricultural and Forest*
775 *Meteorology*, *307*, 108525. https://doi.org/10.1016/j.agrformet.2021.108525
776 Béland, M., & Kobayashi, H. (2021). Mapping forest leaf area density from multiview terrestrial
777 lidar. *Methods in Ecology and Evolution*, *12*(4), 619–633. https://doi.org/10.1111/2041-
778 210X.13550
779 Berninger, F., & Hari, P. (1993). Optimal regulation of gas exchange: Evidence from field data.
780 *Annals of Botany*, *71*(2), 135–140. https://doi.org/10.1006/anbo.1993.1017
781 Bonan, G. B., Williams, M., Fisher, R. A., & Oleson, K. W. (2014). Modeling stomatal
782 conductance in the earth system: Linking leaf water-use efficiency and water transport
783 along the soil-plant-atmosphere continuum. *Geoscientific Model Development*, *7*(5),
784 2193–2222. https://doi.org/10.5194/gmd-7-2193-2014
785 Brodribb, T. J., Holbrook, N. M., Zwieniecki, M. A., & Palma, B. (2005). Leaf hydraulic
786 capacity in ferns, conifers and angiosperms: Impacts on photosynthetic maxima. *New*
787 *Phytologist*, *165*(3), 839–846. https://doi.org/10.1111/j.1469-8137.2004.01259.x
788 Buckley, T. N. (2017). Modeling stomatal conductance. *Plant Physiology*, *174*(2), 572–582.
789 https://doi.org/10.1104/pp.16.01772
790 Campbell, G. S. (1974). A simple method for determining unsaturated conductivity from
791 moisture retention data. *Soil Science*, *117*(6), 311-314. https://doi.org/10.1097/00010694-
792 197406000-00001

Von Caemmerer, S. (2000). *Biochemical models of leaf photosynthesis*. Csiro publishing. https://doi.org/10.1071/9780643103405

Cowan, I. R. (1982). Regulation of Water Use in Relation to Carbon Gain in Higher Plants. In: O. L. Lange, P. S. Nobel, C. B. Osmond, & H. Ziegler (Eds.), *Physiological Plant Ecology II: Water Relations and Carbon Assimilation*, pp. 589–613. Springer. https://doi.org/10.1007/978-3-642-68150-9_18

Cowan, I. R., & Farquhar, G. D. (1977). Stomatal function in relation to leaf metabolism and environment. *Symposia of the Society for Experimental Biology*, *31*, 471–505.

Farquhar, G. D., von Caemmerer, S., & Berry, J. A. (1980a). A biochemical model of photosynthetic CO_2 assimilation in leaves of C_3 species. *Planta*, *149*(1), 78–90. https://doi.org/10.1007/BF00386231

Farquhar, G. D., Schulze, E. D., & Kuppers, M. (1980b). Responses to humidity by stomata of *Nicotiana glauca* L. and *Corylus avellana* L. are consistent with the optimization of carbon dioxide uptake with respect to water loss. *Australian Journal of Plant Physiology*, *7*(3), 315–327. https://doi.org/10.1071/PP9800315

Feldman, A. F., Short Gianotti, D. J., Trigo, I. F., Salvucci, G. D., & Entekhabi, D. (2019). Satellite-based assessment of land surface energy partitioning–soil moisture relationships and effects of confounding variables. *Water Resources Research*, *55*(12), 10657–10677. https://doi.org/10.1029/2019WR025874

Feng, X., Lu, Y., Jiang, M., Katul, G., Manzoni, S., Mrad, A., & Vico, G. (2022). Instantaneous stomatal optimization results in suboptimal carbon gain due to legacy effects. *Plant, Cell & Environment, 45*(11), 3189–3204. https://doi.org/10.1111/pce.14427

Ficklin, D. L., & Novick, K. A. (2017). Historic and projected changes in vapor pressure deficit suggest a continental-scale drying of the United States atmosphere. *Journal of Geophysical Research: Atmospheres*, *122*(4), 2061–2079. https://doi.org/10.1002/2016JD025855

Finnigan, J. J., & Raupach, M. R. (1987). Transfer processes in plant canopies in relation to stomatal characteristics. *Stomatal Function*, 385–429. https://www.cabdirect.org/cabdirect/abstract/19880712530

Fites, J. A., & Teskey, R. O. (1988). CO_2 and water vapor exchange of *Pinustaeda* in relation to stomatal behavior: Test of an optimization hypothesis. *Canadian Journal of Forest Research*, *18*(2), 150–157. https://doi.org/10.1139/x88-024

Franks, P. J., Bonan, G. B., Berry, J. A., Lombardozzi, D. L., Holbrook, N. M., Herold, N., & Oleson, K. W. (2018). Comparing optimal and empirical stomatal conductance models for application in Earth system models. *Global Change Biology*, *24*(12), 5708–5723. https://doi.org/10.1111/gcb.14445

van Genuchten, M. Th. (1980). A closed-form equation for predicting the hydraulic conductivity of unsaturated soils. *Soil Science Society of America Journal*, *44*(5), 892–898. https://doi.org/10.2136/sssaj1980.03615995004400050002x

Green, J. K., Seneviratne, S. I., Berg, A. M., Findell, K. L., Hagemann, S., Lawrence, D. M., & Gentine, P. (2019). Large influence of soil moisture on long-term terrestrial carbon uptake. *Nature*, *565*(7740), 476–479. https://doi.org/10.1038/s41586-018-0848-x

Grieu, P., Guehl, J. M., & Aussenac, G. (1988). The effects of soil and atmospheric drought on photosynthesis and stomatal control of gas exchange in three coniferous species.

Physiologia Plantarum, *73*(1), 97–104. https://doi.org/10.1111/j.1399-3054.1988.tb09199.x

Grossiord, C., Buckley, T. N., Cernusak, L. A., Novick, K. A., Poulter, B., Siegwolf, R. T. W., Sperry, J. S., & McDowell, N. G. (2020). Plant responses to rising vapor pressure deficit. *New Phytologist*, *226*(6), 1550–1566. https://doi.org/10.1111/nph.16485

Hall, A. E., & Schulze, E.-D. (1980). Stomatal response to environment and a possible interrelation between stomatal effects on transpiration and CO_2 assimilation. *Plant, Cell & Environment*, *3*(6), 467–474. https://doi.org/10.1111/1365-3040.ep11587040

Hari, P., Mäkelä, A., & Pohja, T. (2000). Surprising implications of the optimality hypothesis of stomatal regulation gain support in a field test. *Functional Plant Biology*, *27*(1), 77–80. https://doi.org/10.1071/pp99050

Katul, G. G., Palmroth, S., & Oren, R. (2009). Leaf stomatal responses to vapour pressure deficit under current and CO_2-enriched atmosphere explained by the economics of gas exchange. *Plant, Cell & Environment*, *32*(8), 968–979. https://doi.org/10.1111/j.1365-3040.2009.01977.x

Katul, G., Manzoni, S., Palmroth, S., & Oren, R. (2010). A stomatal optimization theory to describe the effects of atmospheric CO_2 on leaf photosynthesis and transpiration. *Annals of Botany*, *105*(3), 431–442. https://doi.org/10.1093/aob/mcp292

Kelliher, F. M., Leuning, R., Raupach, M. R., & Schulze, E.-D. (1995). Maximum conductances for evaporation from global vegetation types. *Agricultural and Forest Meteorology*, *73*(1), 1–16. https://doi.org/10.1016/0168-1923(94)02178-M

Kennedy, D., Swenson, S., Oleson, K. W., Lawrence, D M., Fisher, R., Lola da Costa, A. C., & Gentine, P. (2019). Implementing plant hydraulics in the Community Land Model,

version 5. *Journal of Advances in Modeling Earth Sysntems, 11*(2), 485–513. https://doi.org/10.1029/2018MS001500

Knauer, J., Werner, C., & Zaehle, S. (2015). Evaluating stomatal models and their atmospheric drought response in a land surface scheme: A multibiome analysis. *Journal of Geophysical Research: Biogeosciences*, *120*(10), 1894–1911. https://doi.org/10.1002/2015JG003114

Knauer, J., Zaehle, S., Medlyn, B. E., Reichstein, M., Williams, C. A., Migliavacca, M., De Kauwe, M. G., Werner, C., Keitel, C., Kolari, P., Limousin, J.-M., & Linderson, M.-L. (2018). Towards physiologically meaningful water-use efficiency estimates from eddy covariance data. *Global Change Biology*, *24*(2), 694–710. https://doi.org/10.1111/gcb.13893

Lanning, M., Wang, L., & Novick, K. A. (2020). The importance of cuticular permeance in assessing plant water–use strategies. *Tree Physiology*, *40*(4), 425–432. https://doi.org/10.1093/treephys/tpaa020

Lasslop, G., Reichstein, M., Papale, D., Richardson, A. D., Arneth, A., Barr, A., Stoy, P., & Wohlfahrt, G. (2010). Separation of net ecosystem exchange into assimilation and respiration using a light response curve approach: critical issues and global evaluation. *Global Change Biology, 16*(1), 187–208. https://doi.org/10.1111/j.1365-2486.2009.02041.x

Lawlor, D. W., & Tezara, W. (2009). Causes of decreased photosynthetic rate and metabolic capacity in water-deficient leaf cells: A critical evaluation of mechanisms and integration of processes. *Annals of Botany*, *103*(4), 561–579. https://doi.org/10.1093/aob/mcn244

Leuning, R. (1995). A critical appraisal of a combined stomatal-photosynthesis model for C_3 plants. *Plant, Cell & Environment.*, *18*(4), 339–355. https://doi.org/10.1111/j.1365-3040.1995.tb00370.x

Lin, C., Gentine, P., Huang, Y., Guan, K., Kimm, H., & Zhou, S. (2018). Diel ecosystem conductance response to vapor pressure deficit is suboptimal and independent of soil moisture. *Agricultural and Forest Meteorology*, *250–251*, 24–34. https://doi.org/10.1016/j.agrformet.2017.12.078

Lin, Y.-S., Medlyn, B. E., Duursma, R. A., Prentice, I. C., Wang, H., Baig, S., Eamus, D., de Dios, V. R., Mitchell, P., Ellsworth, D. S., de Beeck, M. O., Wallin, G., Uddling, J., Tarvainen, L., Linderson, M.-L., Cernusak, L. A., Nippert, J. B., Ocheltree, T. W., Tissue, D. T., … Wingate, L. (2015). Optimal stomatal behaviour around the world. *Nature Climate Change*, *5*(5), 459–464. https://doi.org/10.1038/nclimate2550

Lu, Y., Duursma, R. A., Farrior, C. E., Medlyn, B. E., & Feng, X. (2020). Optimal stomatal drought response shaped by competition for water and hydraulic risk can explain plant trait covariation. *New Phytologist*, *225*(3), 1206–1217. https://doi.org/10.1111/nph.16207

Lu, Y. J., Duursma, R. A., & Medlyn, B. E. (2016). Optimal stomatal behaviour under stochastic rainfall. *Journal of Theoretical Biology*, *394*, 160–171. https://doi.org/10.1016/j.jtbi.2016.01.003

Mäkelä, A., Berninger, F., & Hari, P. (1996). Optimal control of gas exchange during drought: Theoretical analysis. *Annals of Botany*, *77*(5), 461–467. https://www.jstor.org/stable/42764687

Manzoni, S., Vico, G., Katul, G., Fay, P. A., Polley, W., Palmroth, S., & Porporato, A. (2011). Optimizing stomatal conductance for maximum carbon gain under water stress: A meta-

905 analysis across plant functional types and climates. *Functional Ecology*, *25*(3), 456–467.
906 https://doi.org/10.1111/j.1365-2435.2010.01822.x
907 Manzoni, S., Vico, G., Palmroth, S., Porporato, A., & Katul, G. (2013). Optimization of stomatal
908 conductance for maximum carbon gain under dynamic soil moisture. *Advances in Water*
909 *Resources*, *62*, 90–105. https://doi.org/10.1016/j.advwatres.2013.09.020
910 Marshall, B. & Biscoe, P. V. (1980). A model for C_3 leaves describing the dependence of net
911 photosynthesis on irradiance, *Journal of Experimental Botany, 31*(1), 29–
912 39. https://doi.org/10.1093/jxb/31.1.29
913 Martinez-Vilalta, J., Poyatos, R., Aguade, D., Retana, J., & Mencuccini, M. (2014). A new look
914 at water transport regulation in plants. *New Phytologist*, *204*(1), 105–115.
915 https://doi.org/10.1111/nph.12912
916 Medlyn, B. E., De Kauwe, M. G., Lin, Y.-S., Knauer, J., Duursma, R. A., Williams, C. A.,
917 Arneth, A., Clement, R., Isaac, P., Limousin, J.-M., Linderson, M.-L., Meir, P., Martin-
918 StPaul, N., & Wingate, L. (2017). How do leaf and ecosystem measures of water-use
919 efficiency compare? *New Phytologist, 216*(3), 758–770.
920 https://doi.org/10.1111/nph.14626.
921 Medlyn, B. E., Duursma, R. A., Eamus, D., Ellsworth, D. S., Colin Prentice, I., Barton, C. V. M.,
922 Crous, K. Y., de Angelis, P., Freeman, M., & Wingate, L. (2012). Reconciling the
923 optimal and empirical approaches to modelling stomatal conductance. *Global Change*
924 *Biology*, *18*(11), 3476–3476. https://doi.org/10.1111/j.1365-2486.2012.02790.x
925 Michaelis, L. & Menten, M. L. (1913). Die kinetik der invertinwirkung. *Biochem. z*, *49*(333-
926 369), 352.

927 Monteith, J. L. (1965). Evaporation and environment. *Symposia of the Society for Experimental*
928 *Biology,* 19, 205–234.
929 Novick, K. A., & Barnes, M. L. (2023). A practical exploration of land cover impacts on surface
930 and air temperature when they are most consequential. *Environmental Research: Climate,*
931 *2*(2), 025007. https://doi.org/10.1088/2752-5295/accdf9
932 Novick, K. A., Ficklin, D. L., Baldocchi, D., Davis, K. J., Ghezzehei, T. A., Konings, A. G.,
933 MacBean, N., Raoult, N., Scott, R. L., Shi, Y., Sulman, B. N., & Wood, J. D. (2022).
934 Confronting the water potential information gap. *Nature Geoscience*, *15*, 158–164.
935 https://doi.org/10.1038/s41561-022-00909-2
936 Novick, K. A., Ficklin, D. L., Stoy, P. C., Williams, C. A., Bohrer, G., Oishi, A. C., Papuga, S.
937 A., Blanken, P. D., Noormets, A., Sulman, B. N., Scott, R. L., Wang, L., & Phillips, R. P.
938 (2016a). The increasing importance of atmospheric demand for ecosystem water and
939 carbon fluxes. *Nature Climate Change, 6*, 1023–1027.
940 https://doi.org/10.1038/nclimate3114
941 Novick, K. A., Konings, A. G., & Gentine, P. (2019). Beyond soil water potential: An expanded
942 view on isohydricity including land-atmosphere interactions and phenology. *Plant, Cell*
943 *& Environment*, 42(6), 1802–1815. https://doi.org/10.1111/pce.13517
944 Novick, K. A., Miniat, C. F., & Vose, J. M. (2016b). Drought limitations to leaf-level gas
945 exchange: Results from a model linking stomatal optimization and cohesion-tension
946 theory. *Plant, Cell & Environment*, *39*(3), 583–596. https://doi.org/10.1111/pce.12657
947 Pastorello, G., Trotta, C., Canfora, E., Chu, H., Christianson, D., Cheah, Y.-W., Poindexter, C.,
948 Chen, J., Elbashandy, A., Humphrey, M., Isaac, P., Polidori, D., Reichstein, M., Ribeca,
949 A., van Ingen, C., Vuichard, N., Zhang, L., Amiro, B., Ammann, C., … Papale, D.

(2020). The FLUXNET2015 dataset and the ONEFlux processing pipeline for eddy covariance data. *Scientific Data*, *7*, 225. https://doi.org/10.1038/s41597-020-0534-3

Paw U, K. T., & Meyers, T. P. (1989). Investigations with a higher-order canopy turbulence model into mean source-sink levels and bulk canopy resistances. *Agricultural and Forest Meteorology*, *47*(2), 259–271. https://doi.org/10.1016/0168-1923(89)90099-3

Sabot, M. E. B., De Kauwe, M. G., Pitman, A. J., Medlyn, B. E., Ellsworth, D. S., Martin-StPaul, N. K., Wu, J., Choat, B., Limousin, J.-M., Mitchell, P. J., Rogers, A., & Serbin, S. P. (2022). One stomatal model to rule them all? Toward improved representation of carbon and water exchange in global models. *Journal of Advances in Modeling Earth Systems*, *14*(4), e2021MS002761. https://doi.org/10.1029/2021MS002761

Sperry, J. S., Venturas, M. D., Anderegg, W. R. L., Mencuccini, M., Mackay, D. S., Wang, Y., & Love, D. M. (2017). Predicting stomatal responses to the environment from the optimization of photosynthetic gain and hydraulic cost. *Plant, Cell & Environment*, *40*(6), 816–830. https://doi.org/10.1111/pce.12852

Stocker, B. D., Zscheischler, J., Keenan, T. F., Prentice, I. C., Peñuelas, J., & Seneviratne, S. I. (2018). Quantifying soil moisture impacts on light use efficiency across biomes. *New Phytologist*, *218*(4), 1430–1449. https://doi.org/10.1111/nph.15123

Thornley, J. H. (1976). *Mathematical Models in Plant Physiology*. Academic Press (Inc.) London, Ltd.

United Nations Environment Programme (1992). World Atlas of Desertification. https://wedocs.unep.org/20.500.11822/42137.

971 Wang, Y., Sperry, J. S., Anderegg, W. R. L., Venturas, M. D., & Trugman, A. T. (2020). A
972 theoretical and empirical assessment of stomatal optimization modeling. *New*
973 *Phytologist*, *227*(2), 311–325. https://doi.org/10.1111/nph.16572
974 Williams, M., Rastetter, E. B., Fernandes, D. N., Goulden, M. L., Wofsy, S. C., Shaver, G. R.,
975 Melillo, J. M., Munger, J. W., Fan, S. M., & Nadelhoffer, K. J. (1996). Modelling the
976 soil-plant-atmosphere continuum in a *Quercus-Acer* stand at Harvard Forest: The
977 regulation of stomatal conductance by light, nitrogen and soil/plant hydraulic properties.
978 *Plant Cell, and Environment.*, *19*(8), 911–927. https://doi.org/10.1111/j.1365-
979 3040.1996.tb00456.x
980 Wolf, A., Anderegg, W. R. L., & Pacala, S. W. (2016). Optimal stomatal behavior with
981 competition for water and risk of hydraulic impairment. *Proceedings of the National*
982 *Academy of Sciences*, *113*(46), E7222–E7230. https://doi.org/10.1073/pnas.1615144113
983 Yamori, W., Hikosaka, K., & Way, D. A. (2014). Temperature response of photosynthesis in C_3,
984 C_4, and CAM plants: Temperature acclimation and temperature adaptation.
985 *Photosynthesis Research*, *119*(1), 101–117. https://doi.org/10.1007/s11120-013-9874-6
986 Yi, K., Maxwell, J. T., Wenzel, M. K., Roman, D. T., Sauer, P. E., Phillips, R. P., & Novick, K.
987 A. (2019). Linking variation in intrinsic water-use efficiency to isohydricity: A
988 comparison at multiple spatiotemporal scales. *New Phytologist*, *221*(1), 195–208.
989 https://doi.org/10.1111/nph.15384
990 Yi, K., Smith, J. W., Jablonski, A. D., Tatham, E. A., Scanlon, T. M., Lerdau, M. T., Novick, K.
991 A., & Yang, X. (2020). High heterogeneity in canopy temperature among co-occurring
992 tree species in a temperate forest. *Journal of Geophysical Research: Biogeosciences,*
993 *125*(12), e2020JG005892. https://doi.org/10.1029/2020JG005892

994 Zhang, Q., Ficklin, D. L., Manzoni, S., Wang, L., Way, D., Phillips, R. P., & Novick, K. A.
995 (2019). Response of ecosystem intrinsic water use efficiency and gross primary
996 productivity to rising vapor pressure deficit. *Environmental Research Letters, 14*(7),
997 074023. https://doi.org/10.1088/1748-9326/ab2603
998 Zhou, S. X., Duursma, R. A., Medlyn, B. E., Kelly, J. W. G., & Prentice, I. C. (2013). How
999 should we model plant responses to drought? An analysis of stomatal and non-stomatal
1000 responses to water stress. *Agricultural and Forest Meteorology*, *182–183*, 204–214.
1001 https://doi.org/10.1016/j.agrformet.2013.05.009
1002 Zhou, S. X., Medlyn, B., Sabate, S., Sperlich, D., & Prentice, I. C. (2014). Short-term water
1003 stress impacts on stomatal, mesophyll and biochemical limitations to photosynthesis
1004 differ consistently among tree species from contrasting climates. *Tree Physiology,*
1005 *34*(10), 1035–1046. https://doi.org/10.1093/treephys/tpu072